The big bang of deep learning in ultrasound-guided surgery: a review

Nima Masoumi, Hassan Rivaz, *Senior member, IEEE*, Ilker Hacihaliloglu, *Member, IEEE*
M. Omair Ahmad, *Fellow, IEEE*, Ingerid Reinertsen, and Yiming Xiao, *Senior member, IEEE*

***Abstract*— Ultrasound (US) imaging is a paramount modality in many image-guided surgeries and percutaneous interventions, thanks to its high portability, temporal resolution, and cost-efficiency. However, due to its imaging principles, US is often noisy and difficult to interpret. Appropriate image processing can greatly enhance the applicability of the imaging modality in clinical practice. Compared with the classic iterative optimization and machine learning approaches, deep Learning (DL) algorithms have shown great performance in terms of accuracy and efficiency for US processing. In this work, we conduct a comprehensive review on deep-learning algorithms in the applications of US-guided interventions, summarize the current trends, and suggest future directions on the topic.**

***Index Terms*— Ultrasound, Deep learning, Surgical guidance, Percutaneous, Intervention**

I. Introduction

ULTRASOUND (US) is a non-ionizing imaging modality that is commonly employed in the clinic, offering 2D, 3D, and 4D data. Although ultrasound transducers are often operated in a free-hand manner by a physician or technician, to ensure image quality, semi-automatic or fully automatic image acquisitions are performed with the assistance of robotic arms in some applications [1]. While avoiding radiation risks, US scanners are portable and cost-effective as opposed to other staple imaging techniques, such as Magnetic Resonance Imaging (MRI) and Computed Tomography (CT). In addition, US offers real-time anatomical and physiological information with great flexibility in applications, such as endoscopic, laparoscopic, transrectal, and transvaginal imaging. In addition to the most commonly seen B-mode contrast for structural imaging, US also provides additional contrasts, including Doppler US for flow imaging and ultrasound elastography computed from raw radio frequency (RF) scans to visualize biophysical properties of tissues. These advantages of US imaging make it a favourable modality for image-guided interventions, where it is used for instrument and biological tissue (e.g., lesions) detection and tracking [2], [3].

Despite multiple benefits, ultrasound still faces several drawbacks primarily as a result of its inherent imaging principle. First, US scans are often noisy and prone to imaging artifacts such as reverberations, refraction, and shadowing, making recognition of anatomy and surgical tools difficult at times. Second, US usually has limited imaging depth, which can restrict the field of view for inspecting the pathological region. Lastly, unlike modalities such as MRI and CT that have standardized planes, the unique image contrast and arbitrary and unfamiliar imaging planes make it challenging to interpret US images. So far, a great number of image processing techniques were proposed to tackle these aforementioned drawbacks, including denoising [4], structure or instrument detection [5], [6], segmentation [7], and image registration [8]–[11]. Traditionally, these techniques heavily rely on time-consuming iterative optimization methods or sub-optimal hand-crafted features for classic machine learning (ML) algorithms. In comparison to conventional techniques, deep Learning (DL)-based methods have shown excellent results in many US processing tasks by leveraging the computing power of modern GPUs [12], [13]. In addition, DL-based methods are faster at inference time especially for large images [14]. With high requirement in accuracy, robustness, and efficiency, deep learning is well suited to facilitate US-guided interventions. To facilitate the readers from diverse backgrounds, we have included a concise introduction to DL in Section S1 of the Supplementary Material.

To date, a number of literature reviews have been conducted on the topic of US-guided interventions. However, most of these previous reviews focus on the survey of clinical applicability of intra-operative US [15]–[17] or related acquisition techniques [18]–[21]. With the great promise of DL techniques to enhance the value of intra-operative US, it is beneficial to provide a comprehensive review on the advancement of DL techniques in therapeutic interventional US. Based on the

Manuscript received 'mentioned the data'. This work was supported in part by the Natural Sciences and Engineering Research Council of Canada (NSERC), Fonds de recherche du Quebec Nature and technologies (FRQNT) and in part by the Regroupment Strategique en Microelectronique du Quebec.

N. Masoumi is with the Department of Electrical Engineering of Concordia University, Montreal, QC, H3G 1M8 (email: n_masoum@encs.concordia.ca)

H. Rivaz is with the Department of Electrical Engineering of Concordia University, Montreal, QC, H3G 1M8 (email: hrivaz@ece.concordia.ca)

I. Hacihaliloglu is with Department of Radiology, Department of Medicine, University of British Columbia, Canada, (email: Ilker.Hacihaliloglu@hli.ubc.ca)

M. O. Ahmad is with the Department of Electrical Engineering of Concordia University, Montreal, QC, H3G 1M8 (email: omair@ece.concordia.ca)

I. Reinertsen is with the Department of Health Research, SINTEF Technology and Society, Trondheim, Norway (email: ingerid.reinertsen@sintef.no)

Y. Xiao is with the Department of Computer Science and Software Engineering of Concordia University, Montreal, QC, H3G 1M8 (email: yiming.xiao@concordia.ca)

survey, we also identify the unmet clinical needs and suggest future research directions in the domain.

II. Literature Selection

We searched the literature using Google Scholar database. The search was performed for publications from January 2015 to December 2022, in the period that DL-based techniques gain popularity in medical imaging. The search criteria "Ultrasound AND (Guided OR Surgery OR Intraoperative) OR (Convolution OR Deep Learning)" was utilized. The papers reviewed are on the technical development and validation of the algorithms, and review articles, case reports, and clinical reports are excluded from the search. The selected papers were carefully screened to ensure they were relevant to US-guided surgery and percutaneous interventions. US-guided diagnosis and biopsies were excluded from our search to focus our review on the therapeutic application of US imaging. The survey resulted in 58 papers. A breakdown of reviewed papers' numbers for each year is shown in Fig 1. A breakdown of the reviewed DL methods in this study is illustrated in Fig 2. To help the readers with their technical developments, we conducted a brief introduction to the common DL models in this survey in Section S2, a summary of the public datasets used in the reviewed papers in Section S3, and a list of reviewed papers' public codes with the web links in Section S4 of the Supplementary Material.

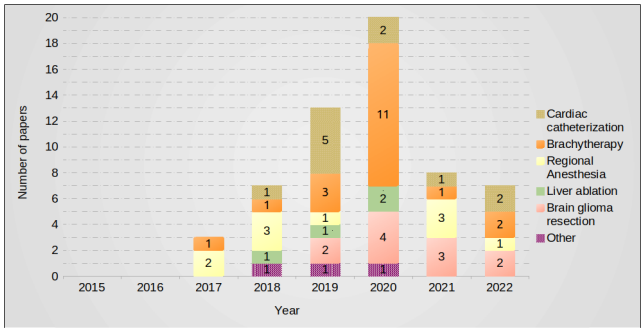

Fig. 1. A breakdown of reviewed papers' numbers for each year is presented. In total, 58 papers were studied. We did not find relevant publications in 2015 and 2016. The number of DL-based approaches in US-guided therapeutic interventions has grown from 2016 until 2020. The drop in publications in the year 2021 is likely due to the COVID-19 pandemic, which may have substantially impacted new data acquisition and research progress in the domain.

III. Clinical Applications

The main clinical applications of the reviewed papers are US-guided cardiac catheterization, brachytherapy, regional anesthesia, liver ablation, and brain glioma resection. While most papers focus on one applications, the others validated the proposed techniques in multiple. Since typically different surgical procedures have different needs, the review for the developed techniques is conducted with respect to their clinical applications.

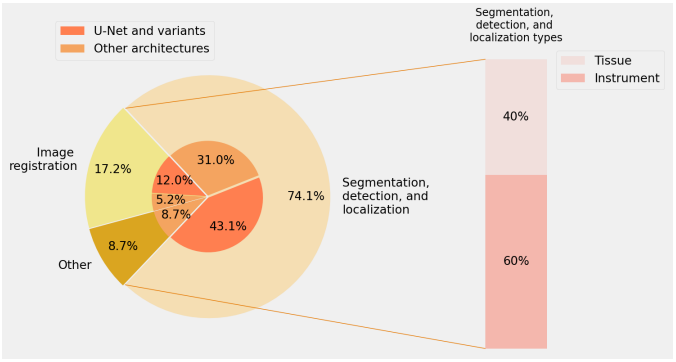

Fig. 2. The methods were classified into three categories: 1. segmentation, detection, and localization, 2. image registration, and 3. other methods. Since U-Net and its variants were employed dominantly more than the other models, we divide the utilized models into: 1. U-Net and variants, and 2. other architectures. Most methods perform segmentation, detection, and localization of medical instruments and target tissues. These methods can be further broken down into tissue and instrument segmentation, detection, and localization. The other methods include the classification of tissues, motion detection, etc.

A. US-guided cardiac catheterization

Catheterization is common in various cardiac interventions, such as angioplasty and heart valve surgery. The catheter has a narrow tubular shape inserted into the patient's artery. The intraoperative X-ray is commonly acquired to localize the catheter. X-ray imaging has risks for interventionalists and patients due to its ionizing radiation. Given this fact, a safer choice, US-guided catheterization, is gaining popularity over intraoperative X-ray. However, locating the catheter in US images, especially near the heart chamber, is challenging, and in the clinic, fast uptake is required. Robust image processing algorithms can automatically detect and localize the catheter in US images. Furthermore, they can also perform voxel/pixel-wise segmentation of the catheter with sub-millimeter precision. Yang *et al.*, in several studies, showed that DL approaches could help the localization and detection of the catheter in US images [22]–[32]. They proposed methods to segment pixels/voxels into catheter and non-catheter classes. The methods were validated in several applications, such as Transcatheter Aortic Valve Implantation (TAVI). The methods are summarized in Table I, and they are primarily validated using private 3D *ex vivo* animal and *in vivo* human datasets. In terms of instrument segmentation, these methods achieved Dice scores up to 70%.

B. US-guided brachytherapy

Brachytherapy is a procedure for treating certain kinds of cancers. In this procedure, small radioactive seeds are placed into the target region of the patient's body using needles or a catheter. The radiation dose of seeds in brachytherapy should be well-localized to the pathological region and spares the adjacent healthy tissues. Therefore, intra-operative guidance, especially with ultrasound has gained the attention of radiation therapists. For prostate brachytherapy, transrectal US (TRUS) is commonly used to guide multiple medical instruments to the targeted region for the correct placement of seeds. Multi-needle localization, detection, and segmentation in US images

TABLE I

A SUMMARY OF DL-BASED METHODS FOR HEART CATHETERIZATION IS PRESENTED. THE METHODS ARE MOSTLY FOCUSED ON CATHETER SEGMENTATION. THE EXAMINED DATASETS ARE ALL PRIVATE.

Reference	Task	Proposed approach	Dataset	Key metric and performance
Yang *et al.* [22]	Catheter localization	A CNN with binary pre-selection of candidate voxels, and applied a Frangi vesselness filter [33] with adaptive thresholding	3D *ex-vivo* porcine heart US	Hausdorff distance of $1.64 \pm 1.82 voxels$
Yang *et al.* [23]	Instrument localization	A modified multi-scale U-Net [34] with a hybrid loss consisting of a contextual loss and a class-balanced focal loss	3D *ex-vivo* porcine heart US and 3D US of *in-vivo* human heart during TAVI operations	Dice score (%) of 69.6 ± 10.9 for *ex-vivo* and 65.8 ± 9.2 for *in-vivo* data
Yang *et al.* [24]	Catheter localization	A 3D U-Net [34] with a cross-entropy focal loss	3D *ex-vivo* porcine heart US	Skeleton error of $1.28mm$
Yang *et al.* [25]	Catheter detection	An early fusion CNN and a late fusion CNN [35] with a weighted cross-entropy loss	3D *ex-vivo* porcine heart US	Position error of $1.7 voxels$
Yang *et al.* [26]	Instrument segmentation	Path-of-interest selection with fusion of a Pyramid-UNet [23] and a direction-fused U-Net which is based on a VGG16 encoder [36]	3D *ex-vivo* porcine heart US and 3D US of *in-vivo* human heart during TAVI operations	Dice score (%) of 70.5 ± 9.2 for *ex-vivo* and 66.5 ± 8.3 for *in-vivo* data
Yang *et al.* [27]	Instrument segmentation	Semi-supervised learning of a deep Q-network using a hybrid loss that consists of uncertainty and contextual constraints	3D *ex-vivo* porcine heart US and 3D US of *in-vivo* human heart during TAVI operations	Dice score (%) of 69.1 ± 7.3 for *ex-vivo* and 68.6 ± 7.9 for *in-vivo* data
Yang *et al.* [28]	Catheter segmentation	Weakly-supervised learning using a ResNet10 encoder [37] with the class attention maps-guided [38] pseudo-label generation	3D *ex-vivo* porcine heart frustum US	Dice score (%) of 65.4 ± 9.7
Yang *et al.* [31]	Catheter segmentation and localization	A direction-fused U-Net which is based on a VGG16 encoder [36]	3D *ex-vivo* porcine heart US	Dice score (%) of 67.7 ± 12.0
Min *et al.* [32]	Catheter segmentation	A VGG encoder [36] with pre-selection of candidate voxels, and applied a Frangi vesselness filter [33]	3D *ex-vivo* porcine heart frustum US	Dice score (%) of 67.3 ± 14

can help accurate insertion of radioactive seeds and potentially improve the treatment efficacy and safety. Ideally, automatic algorithms that perform these tasks should operate in real-time and be robust against image noise and signal distortion in real clinical applications. Zhang *et al.*, in two different studies, proposed multi-needle localization methods using an attention U-Net [34] and a Region-based Convolutional Neural Network (R-CNN) ([39] and [40] respectively). They validated their method on 3D TRUS of patients who underwent High-Dose-Rate (HDR) brachytherapy. A CNN model was developed by Andersen *et al.* [41] to digitize needles in 3D TRUS of prostate HDR brachytherapy patients. Wang *et al.* [42] proposed a U-Net and an additional VGG16-based deep network to segment brachytherapy needles in 3D volumes reconstructed from 2D TRUS slices. Liu *et al.* [43] trained and tested a U-Net model to localize catheter in 3D reconstructed TRUS images taken during several prostate HDR brachytherapies.

Intraoperative prostate segmentation can facilitate the treatment target identification in consideration of patient motion, thus improving the efficiency, safety, and therapeutic outcomes. Girum *et al.* [44], [45] proposed DL approaches using a U-Net and a generative CNN to segment the prostate in 3D reconstructed volumes from 2D TRUS slices. Orlando *et al.* [46] proposed a DL method using a modified U-Net for prostate segmentation on clinically diverse 3D TRUS images. Later, they developed two DL methods using a modified U-Net and a U-Net++ [47], [48], which were trained on 2D TRUS slices [49]. Nevertheless, the methods were tested on 3D TRUS volumetric images. Lei *et al.* [50] proposed DS-V-Net which is a prostate segmentation method using multidirectional V-Net [51]. The popular DS-V-Net achieved the Dice score (%) of 91.9 ± 2.8 in clinical data. A prostate target volume delineation method using residual neural networks for low-dose-rate brachytherapy was developed by Anas *et al.* [52]. The method was validated on 2D TRUS slices using manual segmentation as ground truths. Karimi *et al.* [53], [54] proposed a novel CNN architecture for prostate segmentation in 2D TRUS images. Xiuxiu *et al.* [55] proposed a deep-attentional GAN-based method to improve the resolution of 3D TRUS images. Golshan *et al.* [56] proposed a modified LeNet architecture [57] for radioactive seeds segmentation in 3D TRUS images. This will help confirm the location of implantation and facilitate the procedure that removes these seeds after the treatment period.

Pre-operative MRIs are often acquired for surgical planning in prostate brachytherapy. MRIs generally have sharper images and show better details of the target area than ultrasound. Image registration of intraoperative TRUS with the MRI can help guide the interpretation of the ultrasound scans. Chen *et al.* [58] proposed a DL approach using V-Net and U-Net architectures to segment and register the prostate in MR and TRUS. Zeng *et al.* [59] performed 3D non-rigid registration of MR-TRUS using convolutional and recurrent neural networks.

Brachytherapy is not confined to prostate cancer treatment. Rodgers *et al.* [60] proposed a DL-based method for needle localization in 3D transvaginal US images of interstitial gynecologic HDR brachytherapy. Sun *et al.* [61] generated pseudo-CT images from intraoperative US images of cervical cancer patients for brachytherapy. The DL methods in this section are summarized in Table II. The Dice score, followed by the shaft and needle tip localization errors, are the key metrics for quantitative performance assessment. In general, the algorithms achieved sub-millimeter accuracy in shaft and needle tip localization.

C. US-guided regional anesthesia

Needle-based regional anesthesia is conventionally used in operating rooms. It usually requires an experienced expert to deliver the anesthetic injection. US-guided regional anesthesia

TABLE II

A SUMMARY OF DL-BASED METHODS FOR US-GUIDED BRACHYTHERAPY IS PRESENTED. THE METHODS ARE MOSTLY FOCUSED ON TARGET AND INSTRUMENT SEGMENTATION. PUBLIC DATASETS ARE MARKED WITH "*".

Reference	Task	Proposed Approach	Dataset	Key metrics and Performance
Zhang *et al.* [39]	Multi-needle localization	A deep supervised attention U-Net with a weighted total variation regularization	3D *in-vivo* TRUS of prostate HDR brachytherapy	Shaft localization error of $0.29 \pm 0.23mm$ and needle tip localization error of $0.44 \pm 0.83mm$
Zhang *et al.* [40]	Multi-needle localization	A reformulated large-margin mask R-CNN [62] that is combined with a density-based spatial clustering [63]	3D *in-vivo* TRUS of prostate HDR brachytherapy	Shaft localization error of $0.09 \pm 0.04mm$ and needle tip localization error of $0.33 \pm 0.36mm$
Andersen *et al.* [41]	Digitization of prostate brachytherapy needles	A 3D U-Net architecture [34] with a Dice loss	3D *in-vivo* TRUS volumes reconstructed from 2D slices of prostate HDR brachytherapy	Root-mean-square deviation (RMSD) median (interquartile range) of $0.55 \quad (0.35 - 0.86)$
Wang *et al.* [42]	Needle segmentation	A U-Net followed by a VGG16 network with a categorical cross-entropy loss	3D *in-vivo* TRUS volumes reconstructed from 2D slices of prostate HDR brachytherapy	Resolution of needle trajectories of $0.66mm$ and $0.31mm$ in x and y direction respectively
Liu *et al.* [43]	Catheter localization	A U-Net architecture with a focal Tversky loss function [64]	3D *in-vivo* TRUS volumes reconstructed from 2D slices of prostate HDR brachytherapy	80% within $2mm$ catheter reconstructions
Girum *et al.* [44]	Prostate clinical target-volume boundary detection	A modified U-Net with an integrated regression model using global average pooling	3D *in-vivo* TRUS volumes reconstructed from 2D slices of prostate HDR brachytherapy	Dice score (%) of 88.0 ± 2.0
Girum *et al.* [45]	Prostate clinical target-volume segmentation	A CNN for prior-knowledge generator and a CNN for the segmentation	3D *in-vivo* TRUS volumes reconstructed from 2D slices of prostate HDR brachytherapy, 3D *in-vivo* postoperative CT scans of prostate HDR brachytherapy, and *2D *in-vivo* echocardiography images	Dice score (%) of 96.9 ± 0.9, 95.4 ± 0.9, and 96.3 ± 1.3 for TRUS, CT, and 2D echocardiography images respectively
Orlando *et al.* [46]	Prostate segmentation	A 2D modified U-Net with a Dice loss	3D *in-vivo* TRUS volumes reconstructed from 2D slices of prostate HDR brachytherapy and biopsy	A median (first quartile - third quartile) absolute Dice score (%) of $94.1 \quad (92.6 - 94.9)$
Orlando *et al.* [49]	Prostate segmentation	Trained U-Net and U-Net++ [47], [48] architectures separately using 2D slices	3D *in-vivo* TRUS volumes reconstructed from 2D slices of prostate HDR brachytherapy and biopsy	A median (first quartile - third quartile) absolute Dice score (%) of $94.1 \quad (92.6 - 94.9)$ and $94.0 \quad (92.2 - 95.1)$ for U-Net and U-Net++ respectively
Lei *et al.* [50]	Prostate segmentation	A multidirectional deeply supervised V-Net [51] with a hybrid loss that consists of a binary cross-entropy loss and a batch-based Dice loss	3D *in-vivo* TRUS volumes reconstructed from 2D slices of prostate	Dice score (%) of 91.9 ± 2.8
Anas *et al.* [52]	Clinical target-volume delineation	CNNs based on ResNets [37] and dilated convolution at deeper layers	2D *in-vivo* TRUS of prostate brachytherapy patients	Dice score (%) of 93.67 ± 3.71
Karimi *et al.* [53], [54]	Clinical target-volume segmentation	Sparse subspace clustering [65] of features learned with a convolutional auto-encoder and a modified U-Net architecture	2D *in-vivo* TRUS of prostate brachytherapy patients	Dice score (%) of 93.9 ± 3.5
Xiuxiu *et al.* [55]	Improving US image resolution	Integrating a deeply supervised attention model into a generative adversarial network-based	3D *in-vivo* TRUS volumes reconstructed from 2D slices of prostate	Mean absolute error of 6.5 ± 0.5
Golshan *et al.* [56]	Brachytherapy seeds detection	A LeNet [57] architecture with a cross-entropy loss	3D *in-vivo* volumes reconstructed from 2D original TRUS RF data of prostate brachytherapy patients	Precision, recall, and F1-score (%) of 78.0 ± 8.0, 64.0 ± 10.0, and 70.0 ± 8.0 respectively
Chen *et al.* [58]	MR to TRUS image registration and prostate segmentation	Segmentation-based registration using two weakly-supervised 3D V-Nets [51] for segmentations and a 3D U-Net for the registrations	3D *in-vivo* T2w MRI and 3D *in-vivo* TRUS volumes reconstructed from 2D slices of prostate HDR brachytherapy	Dice score (%) of 97.0 ± 0.0 and 87.0 ± 5.0 for segmented mask and manual contours respectively
Zeng *et al.* [59]	MR to TRUS prostate registration	A modified U-Net [34] and a bidirectional convolutinoal LSTM with a hybrid loss that consists of a bending energy loss and a Dice loss	3D *in-vivo* T2w MRI and 3D *in-vivo* TRUS volumes reconstructed from 2D slices of prostate HDR brachytherapy	Dice score (%) 90.0 ± 4.0
Rodgers *et al.* [60]	Needle localization	A 2D U-Net [83] for 2D data and randomized 3D Hough transforms [66] for 3D data	3D *in-vivo* transvaginal US (TVUS) volumes reconstructed from 2D slices of interstitial gynecological HDR brachytherapy, 2D US slices of phantom brachytherapy, and 2D US slices of ablation therapy	Median position difference (first quartile - third quartile) of $0.27 \quad (0.20 - 0.68)mm$ and $0.79 \quad (0.62 - 0.93)mm$ for 2D and 3D TVUS respectively
Sun *et al.* [61]	Pseudo-CT image synthesis from US	A part of VGG19 [36] network and a hybrid loss that consists of a content loss, a style loss, and a Dice loss	3D *in-vivo* CT scans and 3D *in-vivo* US volumes of cervical cancer patients, additional 3D CT scans of cervical cancer patients, and 3D US phantom data	T-test of structural similarity index between the ground-truth and synthesized CT with $t = 3.22$ and $t = 2.86$ for background and foreground regions respectively

can help the anesthesiologist with the procedure. Detection and localization of the injection needle shaft and tip can be challenging. In 2D US scans, needle tips are occasionally out-of-plane or difficult to spot. Processing raw ultrasound RF data or 3D reconstructed scans is helpful for accurate and reliable needle identification. DL approaches can help with needle localization in US images [67]. Mwikirize *et al.* [68]–[70] developed CNNs in three studies to localize the needle tip in real-time 2D US images. Gao *et al.* [71] proposed a needle segmentation method using a U-Net architecture. Pourtaherian *et al.* [72] proposed a needle tip detection method using orthogonal-plane CNNs. They validated their method on *ex vivo* 3D US images of chicken breast. Later, they developed a method for the localization of needle tips with sub-millimeter accuracy using dilated CNNs [73]. Finally, Maneas *et al.* [80] modified an established residual neural network to improve the axial and lateral resolution of tracked US images for needle localization. They trained their model on synthetic data, and the model was validated on a fetal sheep heart *in vivo* data.

Nerve segmentation in ultrasound scans for US-guided

regional anesthesia can facilitate the practitioners with the procedure. Automatic non-learning methods using Kalman filters could rapidly perform nerve and artery segmentations [74]. Generally, these methods are computationally expensive and require intensive hyperparameter tuning but recent works proposed DL-based techniques to address the drawbacks of classic Kalman filtering [75], [76]. Esmistad *et al.* [77] proposed a technique using U-Net for musculocutaneous, median, ulnar, and radial nerve segmentation during axillary nerve block procedures. Baby *et al.* [78] developed a U-Net model to delineate the brachial plexus in 2D US images. A conditioned U-Net model (www.kaggle.com/harolddiaz1018/unet-cond) was trained by Diaz-Vargas *et al.* [79] to segment ulnar, median, femoral, and sciatic nerves in 2D US slices. The DL methods in this section are summarized in Table III. The shaft and needle tip localization errors are the key metrics for quantitative performance assessment.

D. US-guided liver ablation

Image-guided microwave ablation (MWA) is a promising therapeutic percutaneous intervention that provides a high intralesional temperature. Real-time US imaging techniques can visualize the target for accurate lesion MWA and complete tumour eradication. However, the ablation region margin is not easily detectable in US images. While ablation region delineation is feasible using techniques such as ultrasound elastography [85], we focus our review on DL techniques. Unsupervised classification of target region tissues by leveraging an ML/DL-based method is a candidate approach. Zhang *et al.* [86] utilized the raw ultrasound RF data and trained a CNN network to delineate the ablation region in *ex-vivo* data of the porcine liver. Wang *et al.* [87] proposed a CNN-based method for ablation region detection and monitoring MWA. They performed image registration of US RF data and optical images to boost the accuracy of their method in terms of receiver operating characteristic curves. Kondo *et al.* [88] proposed an out-of-plane motion detection system using CNNs to track the liver tumour movement in ablation therapies.

Ablation needle detection and visualization can help interventionalists during the MWA procedure. Arif *et al.* [89] proposed a real-time bi-planar needle detection and visualization for liver 3D US images. Their method utilizes a U-Net architecture and specific post-processing to perform the needle detection. They execute the registration of images in different time frames acquired from liver phantom and ten patients. The DL methods in this section are summarized in Table IV. Dice score and mean absolute error are the key metrics for quantitative performance assessment.

E. US-guided brain glioma resection

US scanners' portability and cost-effectiveness of US imaging contributed to the growing popularity of intraoperative US acquisition. Spatially tracked ultrasound probes can be calibrated and synced with a neuronavigation system in operating rooms to allow the overlay of real-time US scans with preoperative surgical plans. Practitioners may execute image registration between preoperative images and intraoperative US to update the surgical plan. For instance, in brain glioma surgery, intraoperative US images can be registered to the preoperative MRIs (or intraoperative US images at different time points). Because after surgeons open the dura, the brain tissue can deform up to $18mm$ due to several causes, including gravity, cerebrospinal fluid loss, drug administration, retraction, resection etc [90], [92]. This phenomenon is commonly called brain shift. Brain shift can make the preoperative planning invalid. Therefore, fast registration of preoperative and intraoperative data is crucial. Public datasets, such as the BITE [90] and RESECT [92] databases have greatly facilitated the development of methods for brain-shift correction, including the deep learning approaches. In the CuRIOUS2018 Challenge held in conjunction with MICCAI 2018, the participating teams were asked to register preoperative MRI to intraoperative US images of the RESECT dataset. The challenge results and participating teams' methods are summarized and compared in [91] with most methods using traditional approaches. Canilini *et al.* [93] proposed a DL method using a CNN to segment sulci and falx cerebri in US images. Then, they used the segmentation masks to register intraoperative, preoperative and postoperative US images. The method was tested on BITE and RESECT datasets. Given the fact that these datasets provide manual homologous landmarks, Canilini *et al.* calculated mean Target Registration Error (mTRE) for the quantitative validation of their method. Later, they trained a U-Net architecture to generate segmentation masks of resection cavities [94]. They registered the US volumes using these masks.

Zeineldin *et al.* proposed DL-based methods with U-Net architectures in different studies to register preoperative MRI to intraoperative US images [95]–[97]. They employed MSE Loss for their model training in [95]. Later, they used MSE loss and NCC loss in a comparison study in [96] and NCC loss in [97]. Pirhadi *et al.* [98] employed a Siamese neural network [99] to perform landmark-based registration of pre-resection intraoperative US to post-resection intraoperative US scans.

Finding the precise boundaries of the tumour and its segmentation can assist the surgeons to optimize the resection boundary. Zeineldin *et al.* [100] employed U-Net and TransUNet networks [101] to segment brain tumours in US images. Carton *et al.* [102] proposed a DL-based method with a 3D U-Net architecture to segment the brain tumours of RESECT dataset intraoperative US images. In addition to lesion segmentation, classification of the lesion into different glioma grades or solitary brain metastases can be substantial because the surgical procedures vary for each case. Cepeda *et al.* [103] proposed a DL approach to analyze the candidate lesions in patients who underwent craniotomy. They used B-mode and strain elastography images to correctly classify the lesions as glioblastoma or solitary brain metastases. The DL methods in this section are summarized in Table V.

F. Other clinical applications

Sections III.A-E reviewed the DL approaches in widely studied clinical applications. This section reviews the clinical applications with a few DL-based approaches. Lee *et al.* [105]

TABLE III

A SUMMARY OF DL-BASED METHODS FOR US-GUIDED REGIONAL ANESTHESIA IS PRESENTED. ANESTHESIA NEEDLE TIP LOCALIZATION IS THE FOCUS OF THE MAJORITY OF WORKS. PUBLIC DATASETS ARE MARKED WITH "*".

Reference	Task	Proposed Approach	Dataset	Key metrics and Performance
Mwikirize *et al.* [68]	Real-time needle detection	A region-based CNN [81] and a region-proposal CNN	2D *ex-vivo* US bovine and porcine tissues, and 2D US of bovine/porcine tissues overlaid on lumbosacral spine phantom	Shaft localization error of $0.82^\circ \pm 0.4^\circ$, and needle tip localization error of $0.23 \pm 0.05mm$
Mwikirize *et al.* [69]	Real-time needle tip localization	Needle enhancement followed by a CNN for needle tip classification, and a CNN regression network	2D *ex-vivo* US of bovine, porcine, and chicken tissues overlaid on lumbosacral spine phantom	Needle tip localization error of $0.55 \pm 0.07mm$
Mwikirize *et al.* [70]	Needle tip localization	A novel network that consists of convolutional layers and recurrent layers (CNN-LSTM) with a Mean Squared Error (MSE) loss	2D *ex-vivo* US of bovine, porcine, and chicken tissues overlaid on lumbosacral spine phantom	Needle tip localization error of $0.52 \pm 0.06mm$
Gao *et al.* [71]	Needle localization and enhancement	Beam steering followed by a modified U-Net for segmentation, and a needle fusion algorithm	2D *ex-vivo* US of bovine, porcine, and chicken tissues	Needle tip localization error of $0.29 \pm 0.02mm$
Pourtaherian *et al.* [72]	Needle detection	Two CNNs with shared and independent convolutional filters respectively using a categorical cross-entropy cost	3D *ex-vivo* US of a chicken breast	Precision 83% at 76% recall
Pourtaherian *et al.* [73]	Needle localization	CNNs with dilated convolutions and spatial pyramid pooling features	3D *ex-vivo* US of a porcine leg	Qualitative assessment
Esmistad *et al.* [77]	Nerve segmentation	A modified U-Net	2D *in-vivo* US of volunteers and patients undergoing axillary nerve block procedures	Precision of 88%, 63% 79%, 67%, and 44%, and recall of 0.81, 0.56, 0.71, 0.62, and 0.37 for blood vessel, musculocutaneous nerve, median nerve, ulnar nerve, and radial nerve respectively
Baby *et al.* [78]	Nerve segmentation	A modified U-Net	*2D *in-vivo* US of patients' brachial plexus	Dice score 71%
Diaz-Vargas *et al.* [79]	Peripheral nerve segmentation	A conditioned U-Net with a Dice loss	2D *in-vivo* US of patients' ulnar, median, femoral, and sciatic nerves	Dice score (%) of 70.0 ± 27.0
Maneas *et al.* [80]	Instrumented ultrasonic tracking	ResNet architecture [84] with a L1-loss	2D synthetic US RF data, and 2D *in-vivo* US of fetal sheep heart	Root-mean-square error of 0.15 ± 0.03 for the synthetic data, and signal energy concentration ration of 99.9% for the *in-vivo* data

TABLE IV

A SUMMARY OF DL-BASED METHODS FOR US-GUIDED LIVER ABLATION IS PRESENTED. THE EXAMINED DATASETS ARE ALL PRIVATE.

Reference	Task	Proposed Approach	Dataset	Key metrics and Performance
Zhang *et al.* [86]	Thermal lesion detection	Matched pathology images to US RF data followed by training a CNN with two paths	2D *ex-vivo* US B-mode and RF data liver tissues	Dice score 86.88%
Wang *et al.* [87]	Thermal lesion detection	Image registration of RF data and optical images followed by training a CNN	2D *ex-vivo* US B-mode and RF data, and optical images of the porcine liver tissues	Receiver operating characteristic curve of 0.87
Kondo *et al.* [88]	Tumour motion detection	A VGG16 [36] followed by a U-Net architecture with a hybrid loss	2D US of liver phantom	Mean absolute error of $0.342mm/frame$
Arif *et al.* [89]	Needle detection	Image registration of needles in different time points and needle segmentation using a compressed V-Net [51]	3D *in-vivo* US of liver biopsy patients, and 3D US of puncturing phantoms	Mean absolute error of $1.00mm$ and 2.0° for needle position and orientation respectively

proposed a DL method to classify liver fibrosis. They utilized the data for patients who underwent liver resection surgery. Gillies *et al.* [106] employed a U-Net architecture with a Dice loss to detect general interventional tools in 2D US images. They utilized the datasets of prostate and interstitial gynecologic brachytherapy, liver, and kidney ablations. Wang *et al.* [107] proposed a deep attentive method for prostate segmentation. Their notable approach achieved the Dice score (%) of 90.0 ± 3.0 in the clinical target volume. Hu *et al.* [108] developed an adversarial deformation regularization method for preoperative and procedural TRUS image registration. However, the developed methods of Wang *et al.* [107] and Hu *et al.* [108] have not been designed for a focused application, and they can be used for prostate brachytherapy or prostatectomy.

IV. DISCUSSION AND FUTURE DIRECTIONS

Based on the literature included in the review, deep learning techniques have shown great promise to enhance the value of intra-operative US in surgical interventions. In most of the reviewed papers, the proposed DL methods were compared with traditional methods, where they showed that their techniques could significantly ($p < 0.05$) outperform the traditional ones in the execution time and the evaluation metrics. While segmentation, detection, and localization are the main techniques under development, these also need to be adapted to the application-specific needs and from the current state-of-the arts, we identified a few unmet clinical needs that could be addressed by DL methods in the future. In the literature of brachytherapy, most efforts in DL techniques were dedicated to prostate treatment, even though US-guided brachytherapy was also practised for lung cancer, breast cancer, anal cancer, and abdominal wall metastases. Similarly, deep learning approaches in US-guided ablation is primarily focused on liver while kidney and prostate ablation therapies still have potentials for further technical development. In US-guided tumour resection procedures, similar DL methods can be further adapted for lumpectomy, prostatectomy, tongue cancer resection, laparotomy, pancreatic cancer resection, and bladder cancer resection. Finally, although, US was investigated as an intraoperative imaging tool in orthopedic surgery procedures and complete system with extensive evaluation studies is still

TABLE V

A SUMMARY OF DL-BASED METHODS FOR US-GUIDED BRAIN GLIOMA RESECTION IS PRESENTED. MOST METHODS PERFORM IMAGE REGISTRATION FOR BRAIN SHIFT CORRECTION IN BITE [90] AND RESECT [92] DATASETS. PUBLIC DATASETS ARE MARKED WITH "*".

Reference	Task	Proposed Approach	Dataset	Key metrics and Performance
Canilini *et al.* [93]	Segmentation and registration of US volumes	Segmentation by a modified U-Net [34] and registration of generated masks	*3D *in-vivo* US volumes reconstructed from 2D slices of RESECT [92] and BITE [90] datasets	mTRE of $2.05 \pm 1.12mm$ for RESECT and $2.48 \pm 2.67mm$ for BITE dataset
Canilini *et al.* [94]	Resection cavity segmentation and registration of US volumes	Segmentation by a modified U-Net [34] and registration of generated masks	*3D *in-vivo* US volumes reconstructed from 2D slices of RESECT [92] and BITE [90] datasets	mTRE of $1.21 \pm 0.66mm$ for volumes before and after resection of RESECT, $1.22 \pm 1.20mm$ for volumes before and during resection of RESECT, and $2.38 \pm 2.78mm$ for BITE dataset
Zeineldin *et al.* [95]	MR to US registration	A U-Net architecture with a MSE loss	*3D *in-vivo* US volumes reconstructed from 2D slices and 3D T2-FLAIR MRI of RESECT [92]	Mean squared error of 85
Zeineldin *et al.* [96]	MR to US registration	Two U-Net architecture with MSE and NCC losses respectively	*3D *in-vivo* US volumes reconstructed from 2D slices and 3D T2-FLAIR MR of RESECT [92] and BITE datasets	mTRE of $0.84 \pm 0.16mm$ for RESECT and $1.47 \pm 0.61mm$ for BITE dataset
Zeineldin *et al.* [97]	MR to US registration	A U-Net architecture with a NCC loss	*3D *in-vivo* US volumes reconstructed from 2D slices and 3D T2-FLAIR MRI of RESECT [92] and BITE datasets	mTRE of $0.99 \pm 0.22mm$ for RESECT and $1.68 \pm 0.65mm$ for BITE dataset
Pirhadi *et al.* [98]	Landmark-based US volumes registration	A Siamese network [99] for detecting landmarks with a 2.5D approach [104]	*3D *in-vivo* US volumes reconstructed from 2D slices of RESECT [92] and BITE [90] datasets	mTRE of $1.22 \pm 0.46mm$ for volumes before and after resection of RESECT, $1.11 \pm 0.43mm$ for volumes before and during resection of RESECT, and $1.76 \pm 1.48mm$ for BITE dataset
Zeineldin *et al.* [100]	Brain tumour segmentation	U-Net [83] and TransUNet [101] architectures	*3D *in-vivo* US volumes reconstructed from 2D slices of RESECT [92] dataset	Dice scores (%) of 93.50 and 93.70 for U-Net and TransUNet respectively
Carton *et al.* [102]	Brain tumour segmentation	Three U-Net networks with Dice losses	*3D *in-vivo* US volumes reconstructed from 2D slices of RESECT [92] dataset	Median Dice score (%) of 72.00
Capeda *et al.* [103]	Glioblastoma and solitary brain metastases classification	Employed Inception V3 network from Orange software version 3.26 (University of Ljubljana, Slovenia)	2D *in-vivo* US images of supratentorial tumour patients who underwent craniotomy	Classification accuracy values of 0.79 to 0.94 for B-mode US and 0.84 to 0.97 for elastography data

lacking. Currently, most focus in this domain has been given to developing accurate, robust, and fast bone segmentation [112], [113]. We believe efforts could be directed to propose and evaluate US bone registration approaches [114]. For some domain applications, such as cardiac catheterization, we found that the relevant works were mainly from a handful of labs. This may be due to the availability of clinical resources and collaboration, and it will be beneficial to have more confirmation studies from other research groups in the future. 3D US volume reconstruction is critical for interventional guidance in many clinical applications, such as brain tumour resection [90], [92]. Leblanc *et al.* [109] proposed a US reconstruction technique for peripheral artery imaging. Luo *et al.* [110] leveraged a self-supervised strategy to reconstruct freehand 3D US. Guo *et al.* [111] developed a learning model utilizing self-attention to reconstruct 3D US volumes without tracking. However, most existing techniques use biopsy and diagnostic data to develop the algorithms due to their availability, but they can still be well applied in surgical applications.

Despite the excellent performance, deep learning techniques, including those reviewed in this article still have several drawbacks. First, most algorithms still require large well-annotated data to achieve good performance. This issue can be mitigated by adopting self-supervised and semi-supervised learning to learn feature representations by exploiting unlabeled or partially labeled data. Second, due to coarse and difficult-to-interpret image features as a result of ultrasound's imaging principle, accurate anatomical segmentation is often challenging. DL-based super-resolution and denoising techniques may help enhance the clarity of image features to mitigate the issue. Third, the trained networks often have limited adaptability to new domains (e.g., images from different scanner types or setting). Lastly, most existing algorithms still lack of transparency to help verify the quality of the outcomes. Currently, the lack of large-scale well annotated databases, especially the public repositories poses a bottleneck in algorithm development and fair performance benchmarking, and this also partially contributed to the various under-explored clinical applications as mentioned earlier, besides their application-specific challenges. In interventional applications, well annotated data are often more difficult to obtain, especially with ultrasound. Currently to address the issue, weakly-supervised learning strategies in the reviewed papers have achieved impressive performance [27], [45], [59]. by leveraging categorical or coarse image annotations. With the ability to further reduce the demand for data annotation, unsupervised learning may hold an important role for future developments in interventional applications, but more in-depth investigation is still required. In addition, data augmentation, including simulated US, can help overcome the scarcity of samples. However, the current techniques often fail to provide realistic results. Compared with MRI and CT scans, clear structural delineations in US is more difficult due to the nature of the imaging principles, and often co-registered biopsy, MRI, and CT data may be required when it comes to confirmation of pathological tissue segmentation. As direct contact is needed, for endoscopic applications, image acquisition also demands elaborate setup using surgical navigation systems or robotic assistance. These further complicate the construction of relevant datasets besides the privacy concerns commonly associated

with medical data sharing.

In current literature, convolutional neural networks, especially different variants of U-Net architecture [83] have dominated the reviewed methods. In many applications, to overcome the limited data, CNNs previously trained with other imaging modalties (e.g., natural images) were adapted to the application domain with transfer learning [115]. However, partially due to the lack of public data, general purpose DL algorithms that are more tolerate to scanner types and clinical applications still face major challenges. A few initiatives in MRI and CT DL registration and segmentation, such as the Learn2Reg MICCAI Challenge [116] and the Medical Segmentation Decathlon challenges [117] have attempted to help development these types of algorithms, but there is still a lack of similar endeavors in US. Accessibility to implementations facilitates transferring various architectures to new problems. As many learning-based approaches are highly data-dependent and application-tailored, efforts in the reproducibility of the published algorithms from the research community are still required to ensure the value of the technology in real practice. Several DL architectures are proposed in the reviewed literature. Optimal model selection can largely depend on various factors, including suitability of data types (e.g., static vs. temporal), data dimensions (e.g., 2D vs. 3D), types of the target task (e.g., segmentation, registration, etc.), and requirement of portability (i.e., running on a mobile device, desktop computers, or cloud service). Besides decisions by human experts, automated DL model search has also attracted the attention of the research community [119]. However, the automatic search strategies are still not widely adopted. The more recent Vision Transformers (ViT) has shown better performance in learning long-range spatial dependencies than CNNs, which require more elaborate architecture design to model spatial context of the image [118]. Adoption of ViT and its variants may further improve the accuracy of existing and future DL-methods for intra-operative US.

Interpretability and trustworthiness of deep learning algorithms are crucial for the wide-spread adoption of the end products to the clinic. Conventional algorithms often have a goal-driven black-box design, and in this case, without careful verification, faulty automatic outputs can cause harms to the patients. The latest trend in explainable AI (XAI) intends to improve algorithm transparency through techniques, including spatial attention/activation visualization [120], [121], uncertainty estimation, and multi-task learning [122]. For various surgical applications, XAI methodologies can potentially further detect and explain problematic results from DL-based iUS processing that offer real-time feedback to improve the robustness and reliability of the algorithms, and thus the safety and efficiency of the surgery.

V. Conclusion

This review paper studied 58 DL-based approaches for US-guided heart catheterization, brachytherapy, regional anesthesia, liver ablation, and glioma resection. Near 74% of reviewed methods perform segmentation, detection, and localization of medical instruments and target tissues. Possible research directions for DL-based approaches were discussed in Section IV.

Acknowledgment

This work was supported in part by the Natural Sciences and Engineering Research Council of Canada (NSERC) and in part by the Regroupment Strategique en Microelectronique du Quebec.

References

[1] J.A. Long *et al*., 2012. Development of a novel robot for transperineal needle based interventions: focal therapy, brachytherapy and prostate biopsies. J. Urol. 188, 1369–1374.

[2] A. Pourtaherian *et al*., "Medical Instrument Detection in 3-Dimensional Ultrasound Data Volumes," in *IEEE Transactions on Medical Imaging*, vol. 36, no. 8, pp. 1664-1675, Aug. 2017.

[3] S. G. Yuen et al., (2008). 3D Ultrasound-Guided Motion Compensation System for Beating Heart Mitral Valve Repair. In: Metaxas, D., Axel, L., Fichtinger, G., Székely, G. (eds) Medical Image Computing and Computer-Assisted Intervention - MICCAI 2008. MICCAI 2008. Lecture Notes in Computer Science, vol 5241. Springer, Berlin, Heidelberg.

[4] F. Palhano Xavier de Fontes *et al*., Real time ultrasound image denoising. J Real-Time Image Proc 6, 15–22 (2011).

[5] H.D. Cheng, J. Shan, W. Ju, Y. Guo, and L. Zhang, 2010. Automated breast cancer detection and classification using ultrasound images: A survey. Pattern recognition, 43(1), pp.299-317.

[6] W.Y. Chan, J. Qin, Y. -P. Chui and P. -A. Heng, "A Serious Game for Learning Ultrasound-Guided Needle Placement Skills," in IEEE Transactions on Information Technology in Biomedicine, vol. 16, no. 6, pp. 1032-1042, Nov. 2012,

[7] A. Belaid, D. Boukerroui, Y. Maingourd and J. -F. Lerallut, "Phase-Based Level Set Segmentation of Ultrasound Images," in IEEE Transactions on Information Technology in Biomedicine, vol. 15, no. 1, pp. 138-147, Jan. 2011.

[8] H. Rivaz, S. J. -S. Chen and D. L. Collins, "Automatic Deformable MR-Ultrasound Registration for Image-Guided Neurosurgery," in IEEE Transactions on Medical Imaging, vol. 34, no. 2, pp. 366-380, Feb. 2015.

[9] H. Zhou and H. Rivaz, "Registration of Pre- and Postresection Ultrasound Volumes With Noncorresponding Regions in Neurosurgery," in IEEE Journal of Biomedical and Health Informatics, vol. 20, no. 5, pp. 1240-1249, Sept. 2016.

[10] N. Masoumi, Y. Xiao, H. Rivaz, "ARENA: Inter-modality affine registration using evolutionary strategy", In *IJCARS*, 14, 441–450 (2019). https://doi.org/10.1007/s11548-018-1897-1

[11] N. Masoumi, C. J. Belasso, M. O. Ahmad, H. Benali, Y. Xiao, H. Rivaz, "Multimodal 3D ultrasound and CT in image-guided spinal surgery: public database and new registration algorithms", In *IJCARS*, 16, 555–565 (2021). https://doi.org/10.1007/s11548-021-02323-2

[12] X. Chen, A. Diaz-Pinto, N. Ravikumar, and A.F. Frangi, (2021) Deep learning in medical image registration. Prog Biomed Eng 3:012003

[13] A.K.Z. Tehrani, I.M. Rosado-Mendez, and H. Rivaz, "Robust Scatterer Number Density Segmentation of Ultrasound Images," in IEEE Transactions on Ultrasonics, Ferroelectrics, and Frequency Control, vol. 69, no. 4, pp. 1169-1180, April 2022

[14] G. Balakrishnan, A. Zhao, M. R. Sabuncu, J. Guttag and A. V. Dalca, "VoxelMorph: A Learning Framework for Deformable Medical Image Registration," in IEEE Transactions on Medical Imaging, vol. 38, no. 8, pp. 1788-1800, Aug. 2019

[15] L. Dixon, A. Lim, M. Grech-Sollars, et al. Intraoperative ultrasound in brain tumor surgery: A review and implementation guide. Neurosurg Rev 45, 2503–2515 (2022).

[16] C.O.C.O. Danilo and S. Leanza, 2020. Routine Intraoperative Ultrasound for the Detection of Liver Metastases during Resection of Primary Colorectal Cancer–A Systematic Review. Maedica, 15(2), p.250.

[17] B. Jiao, H. Chen, M. Chen, P. Lu, J. Liu, and C. Chen, 2022. Opioid-sparing effects of ultrasound-guided erector spinae plane block for adult patients undergoing surgery: A systematic review and meta-analysis. Pain Practice, 22(3), pp.391-404.

[18] R. Kessner, D.A. Nakamoto, V. Kondray, S. Partovi, Y. Ahmed, and N. Azar, 2019. Contrast-Enhanced Ultrasound Guidance for Interventional Procedures. Journal of Ultrasound in Medicine, 38(10), pp.2541-2557.

[19] C.P. Nolsøe, A.B. Nolsøe, J. Klubien, H.C. Pommergaard, J. Rosenberg, M.F. Meloni, and T. Lorentzen, 2018. Use of ultrasound contrast agents in relation to percutaneous interventional procedures: a systematic review and pictorial essay. Journal of Ultrasound in Medicine, 37(6), pp.1305-1324.

[20] J.M. DeWitt, M. Arain, K.J. Chang, R. Sharaiha, S. Komanduri, V.R. Muthusamy, and J.H. Hwang, 2021. Interventional endoscopic ultrasound: current status and future directions. Clinical Gastroenterology and Hepatology, 19(1), pp.24-40.

[21] M. Antico, F. Sasazawa, L. Wu, A. Jaiprakash, J. Roberts, R. Crawford, A.K. Pandey, and D. Fontanarosa, 2019. Ultrasound guidance in minimally invasive robotic procedures. Medical image analysis, 54, pp.149-167.

[22] H. Yang, C. Shan, A.F. Kolen, et al. Catheter localization in 3D ultrasound using voxel-of-interest-based ConvNets for cardiac intervention. Int J CARS 14, 1069–1077 (2019).

[23] H. Yang, C. Shan, T. Tan, A.F. Kolen, P.H.N. de With, (2019). Transferring from ex-vivo to in-vivo: Instrument Localization in 3D Cardiac Ultrasound Using Pyramid-UNet with Hybrid Loss. In: , et al. Medical Image Computing and Computer Assisted Intervention - MICCAI 2019. MICCAI 2019. Lecture Notes in Computer Science(), vol 11768. Springer, Cham.

[24] H. Yang, C. Shan, A. F. Kolen and P. H. N. de With, "Automated Catheter Localization in Volumetric Ultrasound Using 3D Patch-Wise U-Net with Focal Loss," 2019 IEEE International Conference on Image Processing (ICIP), 2019, pp. 1346-1350.

[25] H. Yang, C. Shan, A. F. Kolen and P.H.N. de With, "Catheter Detection in 3D Ultrasound Using Triplanar-Based Convolutional Neural Networks," 2018 25th IEEE International Conference on Image Processing (ICIP), 2018, pp. 371-375.

[26] H. Yang, C. Shan, A. Bouwman, A.F. Kolen, and P.H. de With, 2021. Efficient and robust instrument segmentation in 3D ultrasound using patch-of-interest-FuseNet with hybrid loss. Medical Image Analysis, 67, p.101842.

[27] H. Yang, C. Shan, A. Bouwman, L.R.C. Dekker, A.F. Kolen and P. H. N. de With, "Medical Instrument Segmentation in 3D US by Hybrid Constrained Semi-Supervised Learning," in IEEE Journal of Biomedical and Health Informatics, vol. 26, no. 2, pp. 762-773, Feb. 2022.

[28] H. Yang, C. Shan, A.F. Kolen, and P.H. de With, 2022. Weakly-supervised learning for catheter segmentation in 3D frustum ultrasound. Computerized Medical Imaging and Graphics, 96, p.102037.

[29] H. Yang, C. Shan, A.F. Kolen, and P.H.N. de With, (2020). Deep Q-Network-Driven Catheter Segmentation in 3D US by Hybrid Constrained Semi-supervised Learning and Dual-UNet. In: , et al. Medical Image Computing and Computer Assisted Intervention - MICCAI 2020. MICCAI 2020. Lecture Notes in Computer Science(), vol 12261. Springer, Cham.

[30] H. Yang, C. Shan, A. F. Kolen and P. H. N. de With, "Efficient Catheter Segmentation in 3D Cardiac Ultrasound using Slice-Based FCN With Deep Supervision and F-Score Loss," 2019 IEEE International Conference on Image Processing (ICIP), 2019, pp. 260-264.

[31] H. Yang, C. Shan, A. F. Kolen and P. H. N. de With, "Improving Catheter Segmentation and Localization in 3D Cardiac Ultrasound Using Direction-Fused Fcn," 2019 IEEE 16th International Symposium on Biomedical Imaging (ISBI 2019), 2019, pp. 1122-1126.

[32] L. Min, H. Yang, C. Shan, A.F. Kolen, and P.H.N. de With "Feasibility study of catheter segmentation in 3D Frustum ultrasounds by DCNN", Proc. SPIE 11315, Medical Imaging 2020: Image-Guided Procedures, Robotic Interventions, and Modeling, 1131521 (16 March 2020).

[33] A.F. Frangi, W.J. Niessen, K.L. Vincken, and M.A. Viergever, (1998) Multiscale vessel enhancement filtering. In: International conference on medical image computing and computer-assisted intervention, Springer, Berlin, Heidelberg, pp 130–137

[34] Ö. Çiçek, A. Abdulkadir, S.S. Lienkamp, T. Brox, and O. Ronneberger, (2016). 3D U-Net: Learning Dense Volumetric Segmentation from Sparse Annotation. In: Ourselin, S., Joskowicz, L., Sabuncu, M., Unal, G., Wells, W. (eds) Medical Image Computing and Computer-Assisted Intervention - MICCAI 2016. MICCAI 2016. Lecture Notes in Computer Science(), vol 9901. Springer, Cham.

[35] A. Karpathy, G. Toderici , S. Shetty, T. Leung , R. Suk- thankar, and F. Li, "Large-scale video classification with convolutional neural networks," in Proceedings of the IEEE conference on Computer Vision and Pattern Recognition, 2014, pp. 1725-1732

[36] K. Simonyan, and A. Zisserman, 2014. Very deep convolutional networks for large-scale image recognition. arXiv preprint arXiv:1409.1556.

[37] S. Chen, K. Ma, and Y. Zheng, Med3d: Transfer learning for 3d medical image analysis, arXiv:1904.00625 (2019)

[38] B. Zhou, A. Khosla, A. Lapedriza, A. Oliva, and A. Torralba, 2016. Learning deep features for discriminative localization. Proc. IEEE Conf. Comput. Vis. Pattern Recognit. 2921–2929.

[39] Y. Zhang, Y. Lei, R.L. Qiu, T. Wang, H. Wang, A.B. Jani, W.J. Curran, P. Patel, T. Liu, and X. Yang, 2020. Multi-needle localization with attention U-Net in US-guided HDR prostate brachytherapy. Medical physics, 47(7), pp.2735-2745.

[40] Y. Zhang, Z. Tian, Y. Lei, T. Wang, P. Patel, A.B. Jani, W.J. Curran, T. Liu, and X. Yang, 2020. Automatic multi-needle localization in ultrasound images using large margin mask RCNN for ultrasound-guided prostate brachytherapy. Physics in Medicine and Biology, 65(20), p.205003.

[41] C. Andersén, T. Rydén, P. Thunberg, and J.H. Lagerlöf, 2020. Deep learning-based digitization of prostate brachytherapy needles in ultrasound images. Medical physics, 47(12), pp.6414-6420.

[42] F. Wang, L. Xing, H. Bagshaw, M. Buyyounouski, and B. Han, 2020. Deep learning applications in automatic needle segmentation in ultrasound-guided prostate brachytherapy. Medical Physics, 47(9), pp.3797-3805.

[43] D. Liu, DS. Tupor, J. Singh, et al. The challenges facing deep learning–based catheter localization for ultrasound guided high-dose-rate prostate brachytherapy. Med Phys. 2022; 49: 2442– 2451.

[44] K.B. Girum, A. Lalande, R. Hussain, et al. A deep learning method for real-time intraoperative US image segmentation in prostate brachytherapy. Int J CARS 15, 1467–1476 (2020).

[45] K.B. Girum, G. Créhange, R. Hussain, R. et al. Fast interactive medical image segmentation with weakly supervised deep learning method. Int J CARS 15, 1437–1444 (2020).

[46] N. Orlando, D.J. Gillies, I. Gyacskov, C. Romagnoli, D. D'Souza, and A. Fenster, 2020. Automatic prostate segmentation using deep learning on clinically diverse 3D transrectal ultrasound images. Medical physics, 47(6), pp.2413-2426.

[47] Z. Zhou, M.M.R. Siddiquee, N. Tajbakhsh, and J. Liang, 2018 UNet++: a nested U-net architecture for medical image segmentation Lecture Notes in Computer Science (including subseries Lecture Notes in Artificial Intelligence and Lecture Notes in Bioinformatics) 11045 3–11

[48] Z. Zhou, M.M.R. Siddiquee, N. Tajbakhsh, and J. Liang, 2020 UNet++: redesigning skip connections to exploit multiscale features in image segmentation IEEE Trans. Med. Imaging 39 1856–67

[49] N. Orlando, I. Gyacskov, D.J. Gillies, F. Guo, C. Romagnoli, D. D'Souza, D.W. Cool, D.A. Hoover, and A. Fenster, 2022. Effect of dataset size, image quality, and image type on deep learning-based automatic prostate segmentation in 3D ultrasound. Physics in Medicine and Biology, 67(7), p.074002.

[50] Y. Lei, S. Tian, X. He, T. Wang, B. Wang, P. Patel, A.B. Jani, H. Mao, W.J. Curran, T. Liu, and X. Yang, 2019. Ultrasound prostate segmentation based on multidirectional deeply supervised V-Net. Medical physics, 46(7), pp.3194-3206.

[51] F. Milletari, N. Navab, and S.A. Ahmadi. V-Net: fully convolutional neural networks for volumetric medical image segmentation. Proceedings of International Conference on 3D Vision; 2016:565–571.

[52] E.M.A. Anas, et al. (2017). Clinical Target-Volume Delineation in Prostate Brachytherapy Using Residual Neural Networks. In: Descoteaux, M., Maier-Hein, L., Franz, A., Jannin, P., Collins, D., Duchesne, S. (eds) Medical Image Computing and Computer Assisted Intervention - MICCAI 2017. MICCAI 2017. Lecture Notes in Computer Science(), vol 10435. Springer, Cham.

[53] D. Karimi, et al. (2018). Accurate and Robust Segmentation of the Clinical Target Volume for Prostate Brachytherapy. In: Frangi, A., Schnabel, J., Davatzikos, C., Alberola-López, C., Fichtinger, G. (eds) Medical Image Computing and Computer Assisted Intervention – MICCAI 2018. MICCAI 2018. Lecture Notes in Computer Science(), vol 11073. Springer, Cham.

[54] D. Karimi, Q. Zeng, P. Mathur, A. Avinash, S. Mahdavi, I. Spadinger, P. Abolmaesumi, and S.E. Salcudean, 2019. Accurate and robust deep learning-based segmentation of the prostate clinical target volume in ultrasound images. Medical image analysis, 57, pp.186-196.

[55] X. He, Y. Lei, Y. Liu, Z. Tian, T. Wang, W.J. Curran, T. Liu, and X. Yang, "Deep attentional GAN-based high-resolution ultrasound imaging," Proc. SPIE 11319, Medical Imaging 2020: Ultrasonic Imaging and Tomography, 113190B (16 March 2020);

[56] M. Golshan, D. Karimi, S. Mahdavi, J. Lobo, M. Peacock, S.E. Salcudean, and I. Spadinger, 2020. Automatic detection of brachytherapy seeds in 3D ultrasound images using a convolutional neural network. Physics in Medicine and Biology, 65(3), p.035016.

[57] Y. LeCun, et al 1989 Backpropagation Applied to Handwritten Zip Code Recognition Neural Comput. 1 541–51

[58] Y. Chen, L. Xing, L. Yu, W. Liu, R. Pooya Fahimian, T. Niedermayr, H.P. Bagshaw, M. Buyyounouski, and B. Han, 2021. MR to ultrasound

image registration with segmentation-based learning for HDR prostate brachytherapy. Medical Physics, 48(6), pp.3074-3083.

[59] Q. Zeng, Y. Fu, J. Jeong, Y. Lei, T. Wang, H. Mao, A.B. Jani, P. Patel, W.J. Curran, T. Liu, and X. Yang, "Weakly non-rigid MR-TRUS prostate registration using fully convolutional and recurrent neural networks," Proc. SPIE 11313, Medical Imaging 2020: Image Processing, 113132Y (10 March 2020);

[60] J.R. Rodgers, D.J. Gillies, W.T. Hrinivich, I. Gyackov, and A. Fenster, "Automatic needle localization in intraoperative 3D transvaginal ultrasound images for high-dose-rate interstitial gynecologic brachytherapy," Proc. SPIE 11315, Medical Imaging 2020: Image-Guided Procedures, Robotic Interventions, and Modeling, 113150K (16 March 2020);

[61] H. Sun, K. Zhang, R. Fan, W. Xiong, and J. Yang, 2019. Stepwise Local Synthetic Pseudo-CT Imaging Based on Anatomical Semantic Guidance. IEEE Access, 7, pp.168428-168435.

[62] K. He, G. Gkioxari, P. Dollár, and R. Girshick, 2017 Mask R-CNN Proc. of the IEEE Int. Conf. on Computer Vision pp 2961–9

[63] E. Schubert, J. Sander, M. Ester, H.P. Kriegel, and X. Xu, 2017 DBSCAN revisited, revisited: why and how you should (still) use DBSCAN ACM Trans. Database Syst. 42 1–21

[64] N. Abraham, and N.M. Khan. A novel focal Tversky loss function with improved attention U-Net for lesion segmentation; 2018. arXiv:1810.07842v1

[65] E. Elhamifar, R. Vidal, 2013. Sparse subspace clustering: algorithm, theory, and applications. IEEE Trans. Pattern Anal. Mach. Intell. 35 (11), 2765–2781.

[66] W.T. Hrinivich, D.A. Hoover, K. Surry, C. Edirisinghe, J. Montreuil, D. D'Souza, A. Fenster, and E. Wong, "Simultaneous automatic segmentation of multiple needles using 3D ultrasound for high-dose-rate prostate brachytherapy," Med. Phys. 44(4), 1234–1245 (2017).

[67] D. Viderman, M. Dossov, S. Seitenov, and M.H. Lee, 2022. Artificial intelligence in ultrasound-guided regional anesthesia: A scoping review. Frontiers in Medicine, p.3037.

[68] C. Mwikirize, J.L. Nosher, and I. Hacihaliloglu, Convolution neural networks for real-time needle detection and localization in 2D ultrasound. Int J CARS 13, 647–657 (2018).

[69] C. Mwikirize, J.L. Nosher, I. Hacihaliloglu, (2019). Single Shot Needle Tip Localization in 2D Ultrasound. In: , et al. Medical Image Computing and Computer Assisted Intervention - MICCAI 2019. MICCAI 2019. Lecture Notes in Computer Science(), vol 11768. Springer, Cham.

[70] C. Mwikirize, A.B. Kimbowa, S. Imanirakiza, et al. Time-aware deep neural networks for needle tip localization in 2D ultrasound. Int J CARS 16, 819–827 (2021).

[71] J. Gao, P. Liu, G.D. Liu, et al. Robust needle localization and enhancement algorithm for ultrasound by deep learning and beam steering methods. JOURNAL OF COMPUTER SCIENCE AND TECHNOLOGY 36(2): 334–346 Mar. 2021.

[72] A. Pourtaherian, et al. (2017). Improving Needle Detection in 3D Ultrasound Using Orthogonal-Plane Convolutional Networks. In: Descoteaux, M., Maier-Hein, L., Franz, A., Jannin, P., Collins, D., Duchesne, S. (eds) Medical Image Computing and Computer-Assisted Intervention - MICCAI 2017. MICCAI 2017. Lecture Notes in Computer Science(), vol 10434. Springer, Cham.

[73] A. Pourtaherian, N. Mihajlovic, F.G. Zanjani, S. Zinger, G.C. Ng, H.H. Korsten, and P.H. De With, 2018, October. Localization of partially visible needles in 3D ultrasound using dilated CNNs. In 2018 IEEE International Ultrasonics Symposium (IUS) (pp. 1-4). IEEE.

[74] E. Smistad and F. Lindseth, "Real-Time Automatic Artery Segmentation, Reconstruction and Registration for Ultrasound-Guided Regional Anaesthesia of the Femoral Nerve," in IEEE Transactions on Medical Imaging, vol. 35, no. 3, pp. 752-761, March 2016.

[75] G. Revach *et al.*, "KalmanNet: Neural Network Aided Kalman Filtering for Partially Known Dynamics," in IEEE Transactions on Signal Processing, vol. 70, pp. 1532-1547, 2022.

[76] A. Arjas *et al.*, "Neural Network Kalman Filtering for 3-D Object Tracking From Linear Array Ultrasound Data," in IEEE Transactions on Ultrasonics, Ferroelectrics, and Frequency Control, vol. 69, no. 5, pp. 1691-1702, May 2022.

[77] E. Smistad, K.F. Johansen, D.H. Iversen, and I. Reinertsen, 2018. Highlighting nerves and blood vessels for ultrasound-guided axillary nerve block procedures using neural networks. Journal of Medical Imaging, 5(4), p.044004.

[78] M. Baby, and A.S. Jereesh, 2017, April. Automatic nerve segmentation of ultrasound images. In 2017 International Conference of Electronics, Communication and Aerospace Technology (ICECA) (Vol. 1, pp. 107-112). IEEE

[79] H.M. Díaz-Vargas, C.A. Jimenez-Castaño, D.A. Cárdenas-Peña, O.D. Aguirre-Ospina, A.A. Orozco-Gutierrez, (2021). Peripheral Nerve Segmentation in Ultrasound Images Using Conditioned U-Net. In: Hernández Heredia, Y., Milián Núñez, V., Ruiz Shulcloper, J. (eds) Progress in Artificial Intelligence and Pattern Recognition. IWAIPR 2021. Lecture Notes in Computer Science(), vol 13055. Springer, Cham.

[80] E. Maneas et al., "Deep Learning for Instrumented Ultrasonic Tracking: From Synthetic Training Data to In Vivo Application," in IEEE Transactions on Ultrasonics, Ferroelectrics, and Frequency Control, vol. 69, no. 2, pp. 543-552, Feb. 2022,

[81] R. Girshick, (2015) Fast R-CNN. In: Proceedings of IEEE interna- tional conference on computer vision, pp 1440–148

[82] C. Mwikirize, J.L. Nosher, and I. Hacihaliloglu: Learning needle tip localization from digital subtraction in 2D ultrasound. Int. J. CARS 14(6), 1017–1026 (2019)

[83] O. Ronneberger, P. Fischer, and T. Brox, (2015). U-Net: Convolutional Networks for Biomedical Image Segmentation. In: Navab, N., Hornegger, J., Wells, W., Frangi, A. (eds) Medical Image Computing and Computer-Assisted Intervention – MICCAI 2015. MICCAI 2015. Lecture Notes in Computer Science(), vol 9351. Springer, Cham.

[84] K. He, X. Zhang, S. Ren, and J. Sun, "Deep residual learning for image recognition," in Proc. IEEE Conf. Comput. Vis. Pattern Recognit.(CVPR), Jun. 2016, pp. 770–778.

[85] H. Rivaz, et al. (2008). Ablation Monitoring with Elastography: 2D In-vivo and 3D Ex-vivo Studies. In: Metaxas, D., Axel, L., Fichtinger, G., Székely, G. (eds) Medical Image Computing and Computer-Assisted Intervention – MICCAI 2008. MICCAI 2008. Lecture Notes in Computer Science, vol 5242. Springer, Berlin, Heidelberg.

[86] S. Zhang et al., "Detection and Monitoring of Thermal Lesions Induced by Microwave Ablation Using Ultrasound Imaging and Convolutional Neural Networks," in IEEE Journal of Biomedical and Health Informatics, vol. 24, no. 4, pp. 965-973, April 2020,

[87] M. Wang et al., "Detection and Monitoring of Microwave Ablation by Ultrasound Imaging Based on Convolutional Neural Network," 2020 IEEE International Ultrasonics Symposium (IUS), 2020, pp. 1-3,

[88] R. Kondo, N. Koizumi, Y. Nishiyama, N. Matsumoto, and K. Numata, 2018, June. Out-of-plane motion detection system using convolutional neural network for US-guided radiofrequency ablation therapy. In 2018 15th International Conference on Ubiquitous Robots (UR) (pp. 729-731). IEEE

[89] M. Arif, A. Moelker, and T. van Walsum, 2019. Automatic needle detection and real-time bi-planar needle visualization during 3D ultrasound scanning of the liver. Medical image analysis, 53, pp.104-110.

[90] L. Mercier, R.F.D. Maestro, K. Petrecca, D. Araujo, C. Haegelen, and D.L. Collins, 'Online database of clinical MR and ultrasound images of brain tumors," In *Medical Physics*, vol. 39, p. 3253, 2012.

[91] Y. Xiao, H. Rivaz, M. Chabanas, M. Fortin, I. Machado, Y. Ou, M.P. Heinrich, J.A. Schnabel, X. Zhong, A. Maier, and W. Wein, 2019. Evaluation of MRI to ultrasound registration methods for brain shift correction: the CuRIOUS2018 challenge. IEEE transactions on medical imaging, 39(3), pp.777-786.

[92] Y. Xiao, M. Fortin, G. Unsgård, H. Rivaz, and I. Reinertsen, "REtro-Spective Evaluation of Cerebral Tumors (RESECT): A clinical database of pre-operative MRI and intra-operative ultrasound in low-grade glioma surgeries", In *Medical Physics*, 2017, 44: 3875-3882. https://doi.org/10.1002/mp.12268

[93] L. Canalini, J. Klein, S. Miller, et al. Segmentation-based registration of ultrasound volumes for glioma resection in image-guided neurosurgery. Int J CARS 14, 1697–1713 (2019).

[94] L. Canalini, J. Klein, D. Miller, and R. Kikinis, 2020. Enhanced registration of ultrasound volumes by segmentation of resection cavity in neurosurgical procedures. International journal of computer assisted radiology and surgery, 15(12), pp.1963-1974

[95] R.A. Zeineldin, M.E. Karar, J. Coburger, C.R. Wirtz, F. Mathis-Ullrich, and O. Burgert, 2020. Towards automated correction of brain shift using deep deformable magnetic resonance imaging-intraoperative ultrasound (MRI-iUS) registration. Current directions in biomedical engineering, 6(1).

[96] R.A. Zeineldin, M.E. Karar, Z. Elshaer, M. Schmidhammer, J. Coburger, C.R. Wirtz, O. Burgert, and F. Mathis-Ullrich, 2021. iRegNet: non-rigid registration of MRI to interventional US for brain-shift compensation using convolutional neural networks. IEEE Access, 9, pp.147579-147590.

[97] R.A. Zeineldin, M.E. Karar, F. Mathis-Ullrich, O. Burgert. A Hybrid Deep Registration of MR Scans to Interventional Ultrasound for Neurosurgical Guidance. In: Lian, C., Cao, X., Rekik, I., Xu, X., Yan, P. (eds) Machine Learning in Medical Imaging. MLMI 2021. Lecture Notes in Computer Science(), vol 12966. Springer, Cham.

[98] A. Pirhadi, S. Salari, M.O. Ahmad, H. Rivaz, and Y. Xiao, 2022. Robust landmark-based brain shift correction with a Siamese neural network in ultrasound-guided brain tumor resection. International Journal of Computer Assisted Radiology and Surgery, pp.1-8.

[99] L. Bertinetto, J. Valmadre, J.F. Henriques, A. Vedaldi, P.H. Torr, (2016) Fully-convolutional Siamese networks for object tracking. In: European conference on computer vision. Springer, pp 850–865

[100] R.A. Zeineldin, A. Pollok, T. Mangliers, M.E. Karar, F. Mathis-Ullrich, and O. Burgert, 2022. Deep automatic segmentation of brain tumours in interventional ultrasound data. Current directions in biomedical engineering, 8(1), pp.133-137.

[101] J. Chen, Y. Lu, Q. Yu, X. Luo, E. Adeli, Y. Wang, L. Lu, A.L. Yuille, and Y. Zhou, 2021. Transunet: Transformers make strong encoders for medical image segmentation. arXiv preprint arXiv:2102.04306.

[102] F.X. Carton, M. Chabanas, B.K. Munkvold, I. Reinertsen, and J.H. Noble, 2020, March. Automatic segmentation of brain tumor in intraoperative ultrasound images using 3D U-Net. In Medical Imaging 2020: Image-Guided Procedures, Robotic Interventions, and Modeling (Vol. 11315, pp. 190-195). SPIE

[103] S. Cepeda, S. García-García, I. Arrese, G. Fernández-Pérez, M. Velasco-Casares, M. Fajardo-Puentes, T. Zamora, and R. Sarabia, 2021. Comparison of intraoperative ultrasound B-mode and strain elastography for the differentiation of glioblastomas from solitary brain metastases. An automated deep learning approach for image analysis. Frontiers in Oncology, 10, p.590756.

[104] M.P. Heinrich, and L. Hansen, (2020) Highly accurate and memory efficient unsupervised learning-based discrete CT registration using 2.5D displacement search. In: International conference on medical image computing and computer-assisted intervention. Springer, pp 190–200

[105] J.H. Lee, I. Joo, T.W. Kang, Y.H. Paik, D.H. Sinn, S.Y. Ha, K. Kim, C. Choi, G. Lee, J. Yi, and W.C. Bang, 2020. Deep learning with ultrasonography: automated classification of liver fibrosis using a deep convolutional neural network. European radiology, 30(2), pp.1264-1273.

[106] D.J. Gillies, J.R. Rodgers, I. Gyacskov, P. Roy, N. Kakani, D.W. Cool, and A. Fenster, 2020. Deep learning segmentation of general interventional tools in two-dimensional ultrasound images. Medical Physics, 47(10), pp.4956-4970.

[107] Y. Wang et al., "Deep Attentive Features for Prostate Segmentation in 3D Transrectal Ultrasound," in IEEE Transactions on Medical Imaging, vol. 38, no. 12, pp. 2768-2778, Dec. 2019,

[108] Y. Hu *et al.*, (2018). Adversarial Deformation Regularization for Training Image Registration Neural Networks. In Medical Image Computing and Computer Assisted Intervention - MICCAI 2018. MICCAI 2018. Lecture Notes in Computer Science, vol 11070. Springer, Cham.

[109] T. Leblanc *et al.*, Stretched reconstruction based on 2D freehand ultrasound for peripheral artery imaging. Int J CARS 17, 1281–1288 (2022).

[110] M. Luo *et al.*, (2022). Deep Motion Network for Freehand 3D Ultrasound Reconstruction. In MICCAI 2022. Lecture Notes in Computer Science, vol 13434. Springer, Cham.

[111] H. Guo, S. Xu, B. Wood, and P. Yan, "Sensorless Freehand 3D Ultrasound Reconstruction via Deep Contextual Learning," in MICCAI 2020, pp. 463–472.

[112] P.U. Pandey, N. Quader, P. Guy, R. Garbi, and A.J. Hodgson, 2020. Ultrasound bone segmentation: a scoping review of techniques and validation practices. Ultrasound in Medicine and Biology, 46(4), pp.921-935.

[113] I. Hacihaliloglu, 2017. Ultrasound imaging and segmentation of bone surfaces: A review. Technology, 5(02), pp.74-80.

[114] S. Schumann, (2016). State of the Art of Ultrasound-Based Registration in Computer Assisted Orthopedic Interventions. In: Zheng, G., Li, S. (eds) Computational Radiology for Orthopaedic Interventions. Lecture Notes in Computational Vision and Biomechanics, vol 23. Springer, Cham.

[115] G. Ayana, K. Dese, and S.W. Choe, 2021. Transfer learning in breast cancer diagnoses via ultrasound imaging. Cancers, 13(4), p.738.

[116] A. Hering et al., "Learn2Reg: comprehensive multi-task medical image registration challenge, dataset and evaluation in the era of deep learning," in IEEE Transactions on Medical Imaging, 2022.

[117] M. Antonelli, A. Reinke, S. Bakas, et al. The Medical Segmentation Decathlon. Nat Commun 13, 4128 (2022).

[118] S. Khan, M. Naseer, M. Hayat, S.W. Zamir, F.S. Khan, and M. Shah, 2022. Transformers in vision: A survey. ACM computing surveys (CSUR), 54(10s), pp.1-41.

[119] E. Thomas, J. H. Metzen, and F. Hutter. "Neural architecture search: A survey." The Journal of Machine Learning Research 20.1 (2019): 1997-2017.

[120] A. Rasoulian, S. Salari, and Y. Xiao, (2022). Weakly Supervised Intracranial Hemorrhage Segmentation Using Hierarchical Combination of Attention Maps from a Swin Transformer. In: , et al. Machine Learning in Clinical Neuroimaging. MLCN 2022. Lecture Notes in Computer Science, vol 13596. Springer, Cham.

[121] R.R. Selvaraju, M. Cogswell, A. Das, R. Vedantam, D. Parikh, and D. Batra, 2017. Grad-cam: Visual explanations from deep networks via gradient-based localization. In Proceedings of the IEEE international conference on computer vision (pp. 618-626).

[122] D. Minh, H.X. Wang, Y.F. Li, et al. Explainable artificial intelligence: a comprehensive review. Artif Intell Rev 55, 3503–3568 (2022).